A non-classical route of efficient plant uptake verified with fluorescent nanoparticles and root adhesion forces investigated using AFM

sandeep sharma
Institute of Nano Science and Technology
Mohd. Muddassir
CSIR-institute of microbial technology
Saraladevi Muthusamy
Lund University
Pardeep Kumar Vaishnav
All India Institute of Medical Sciences
Manish Singh
Institute of nano science and technology
Selvaraju Kanagarajan (selvaraju.kanagarajan@slu.se)
https://orcid.org/0000-0003-4341-9322
Deepak Sharma
CSIR-institute of microbial technology
Vijayakumar Shanmugham
Institute of Nano Science and Technology https://orcid.org/0000-0001-7117-5631

Research

Keywords: Plant nanonutrients, nanoagriculture, crop hydrophobic uptake

Posted Date: May 10th, 2020

DOI: https://doi.org/10.21203/rs.3.rs-26743/v1

Version of Record: A version of this preprint was published at Scientific Reports on November 6th, 2020.
See the published version at https://doi.org/10.1038/s41598-020-75685-3.

A non-classical route of efficient plant uptake verified with fluorescent nanoparticles and root adhesion forces investigated using AFM

Sandeep Sharma,[1] Mohd. Muddassir,[2] Saraladevi Muthusamy,[3] Pardeep Kumar Vaishnav,[4] Manish Singh,[1] Selvaraju Kanagarajan,[5]* Deepak Sharma[2] and Vijayakumar Shanmugam[1]*

[1]Institute of Nano Science and Technology, Habitat Centre, Phase- 10, Sector- 64, Mohali, Punjab – 160062, India.

[2]CSIR-Institute of Microbial Technology, Chandigarh, India.

[3]Applied Microbiology, Department of Chemistry, Lund University, Sweden.

[4]Microscopy division, AIIMS, New Delhi.

[5]Department of Plant Breeding, Swedish University of Agricultural Sciences, Alnarp, Sweden.

***Corresponding Authors**

Selvaraju Kanagarajan (selvaraju.kanagarajan@slu.se); Vijayakumar Shanmugam (vijayakumarshanmugham@gmail.com).

Abstract

- **Background**: Classical plant uptake is limited to water soluble or dispersible material. Further, the knowledge of adhesion and uptake of hydrophobic particles is limited to mammalian and bacterial cells, but not studied in plants; so here first time, we tested the fate of hydrophobic particles (oleylamine coated $Cu_{2-x}Se$ NPs) in comparison to hydrophilic particles (chitosan coated $Cu_{2-x}Se$ NPs) by treatment on the plant roots and studied the mechanism behind the uptake. Further, $Cu_{2-x}Se$ NPs are one of the most popular nanomaterial which has been used in various fields *viz.,* electrical, semiconductor industries, biomedicine and in sensing. However, the effects of these NPs on plants have been seldom studied. So here, along with polarity-based uptake, the toxicity of these NPs is investigated in a model plant, tomato.
- **Results**: Here, hydrophobic NPs have been found to be ~1.3 times more efficient than hydrophilic NPs in tomato plant root penetration. An atomic force microscopy (AFM) adhesion force experiment confirms that hydrophobic NPs experience non-spontaneous yet energetically favourable root trapping and penetration. Further, a relative difference in the hydrophobic vs. hydrophilic NPs movement from the roots to shoots is observed and found related to the change in the protein corona identified by 2D-PAGE analysis. Finally, the toxicity assays showed that $Cu_{2-x}Se$ NPs lead to non-significant toxicity as compared to control.
- **Conclusions**: The enhanced uptake of hydrophobic NPs by the roots proves that non-classical forced penetration is more efficient. Hence, this enhanced uptake and sedentary behaviour of hydrophobic NPs in root can be adopted for eco-friendly leach-proof fertilizer application.

Keywords

Plant nanonutrients, nanoagriculture, crop hydrophobic uptake

Background

Plants have evolved slowly through natural selection processes, which have been rapidly increased by biotechnology for human requirements [1]. Recently, in phytonanotechnology, plants have been tuned positively by the intrinsic properties of nanoparticles (NPs), such as

electron conductivity (improved the electron transport rate of photosystem 1 by 8.8%) [2], ROS scavenging [3], water/nutrient retention/supply [4], and genetic manipulation [5,6]. Furthermore, NPs loaded with the chemical active ingredients have also extended the scope of microsurgery in plants through triggered release [7–9]. To understand the physiological consequences [10–12], a comparison of the vascular uptake of NPs was carried out. Interestingly, some aquatic plants showed greater uptake of NPs than ions [13].

Classical plant uptake mechanism includes passive spontaneous diffusion, mass flow, ion exchange and active energy intensive carrier-assisted method [14]. In NPs uptake also, similar passive mechanisms were identified in metals (M) [15–17], metal oxides (MO) [18,19], chalcogenides (MS) [20], and carbon materials [2,5,21]. Even carrier mediated transport of NPs within the plant cell to different organelles were also documented [22]. These penetrating NPs were found to be transported both by symplastic and apoplastic modes and have shown xylem and phloem transport [23]. Furthermore, the role of NPs coating, such as with/without citrate [24], and surface charges [25,26] on plant uptake behaviour was also studied.

For efficient plant-gene manipulation with NPs, forced-injection strategies were developed by us and others, but such pressure assisted delivery systems are not easy to adopt in large-scale field applications [27,28]. Hence, we envisage that similar forced injection method in large-scale may be feasible by having hydrophobic surface modification. Both theoretically and experimentally, hydrophobicity in combination with mildly hydrophilic groups was found to show excellent adhesion of water drop even with a tilt of 180° [29–33]. Similarly, hydrophobic NPs were found to be more easily penetrate lipid membranes in aqueous media [34]. This enhanced adhesion by hydrophobicity, motivated us to test the plant uptake efficiency between hydrophobic *vs.* hydrophilic NPs.

For this comparison, intensely fluorescent $Cu_{2-X}Se$ NPs were used, which are nontoxic, unlike cadmium particles. Owing to the antioxidant role of selenium based amino acid [35], and recommendation of copper and selenium as plants micronutrient fairly convince us to use $Cu_{2-X}Se$ NPs as the model particle [36]. Furthermore, $Cu_{2-X}Se$ is an isoform of the stable sulphides chalcogenide-family antidote that is preferentially formed by plants to overcome metal ion and metal oxide toxicity [37–39]. Here, the $Cu_{2-X}Se$ NPs are synthesized in oleylamine (CS@OA) as reported before, which gives them hydrophobicity. To have an equivalent hydrophilic particle,

the as-prepared $Cu_{2-x}Se$ NPs were coated with amphiphilic biopolymer chitosan (CS@CH) and transferred into hydrophilic [40–42]. To test the uptake kinetics, economically valuable model plant physiology plant i.e., tomato was used [43,44]. Additionally, to our knowledge for the first time, force distance measurements has been conducted using AFM with the NPs modified tips against root to understand the adhesion dependence.

Results and discussion

Synthesis and characterization

To study the effects of NPs surface polarity on plant uptake, as-prepared hydrophobic $Cu_{2-x}Se$ NPs with oleylamine coating and hydrophilic $Cu_{2-x}Se$ NPs with chitosan coating were tested against the model plant *viz*., tomato. The X-ray diffraction (XRD) pattern of the as-prepared oleylamine coated $Cu_{2-x}Se$ NPs (Fig. 1A) shows diffraction peaks at 26.77, 44.72, 53.03 and 65.27° that match the (111), (220), (311) and (400) planes of face-centred-cubic $Cu_{2-x}Se$ (JCPDS 06-0680) (for brevity, this material will be denoted as CS@OA). Following the XRD confirmation of the as-prepared $Cu_{2-x}Se$ NPs, to develop hydrophilic substitutes of the same, $Cu_{2-x}Se$ NPs were coated with chitosan (for brevity, this material will be denoted as CS@CH). The chitosan coating was difficult to confirm by fourier transform infrared (FT-IR) spectrophotometer, as the oleylamine signals overlap with the chitosan signals w.r.t N-H bending at 1381 cm^{-1} and 1625 cm^{-1} and C-N bonding/N-H stretching at 3400 cm^{-1} (Additional file 1: Fig. S1) [45–47]. However, the visual observation of the CS@CH NPs dispersed well in distilled water compared to the complete precipitation of the CS@OA NPs in distilled water confirms the coating (Additional file 1: Fig. S2). Furthermore, to quantify the change in the NPs surface polarity, the material before and after chitosan coating was drop cast onto glass, and the contact angle was measured. The contact angle of the CS@OA NPs has been found to be 142° (this is close to the value of superhydrophobicity (150°) [48,49], which after chitosan coating in CS@CH NPs decreased to 123° (inset in Fig. 1C, D). This chitosan coating has not been found to affect the absorbance intensity (Additional file 1: Fig. S3). The intense fluorescence of the $Cu_{2-x}Se$ NPs needed to be retained for the tracking of the NPs through confocal imaging. Hence, the photoluminescence (PL) spectra of CS@OA NPs and CS@CH NPs were measured in 1:1 ratio of ethanol: water mixture at 370 nm excitation wavelength. The spectra show no major compromises in signal intensity after coating, which ensures its insignificance on the imaging

(Fig. 1B). The transmission electron microscope (TEM) image of the CS@OA NPs shows monodisperse NPs with a size distribution of approximately 15±8 nm (Fig. 1C). The high resolution (HR) TEM (HR-TEM) (inset in Fig. 1C) shows a lattice spacing of 0.33 nm, which corresponds to the (111) plane of $Cu_{2-x}Se$ NPs. The TEM image after chitosan coating shows that the size and shape of the NPs is stable (Fig. 1D). The size of CS@CH NPs has been found in the range from 15 nm to 30 nm. In agreement with the higher molecular weight of chitosan, the hydrodynamic peak size of the CS@CH NPs has been found to be 9 nm greater than that of the CS@OA NPs (Additional file 1: Fig. S4).

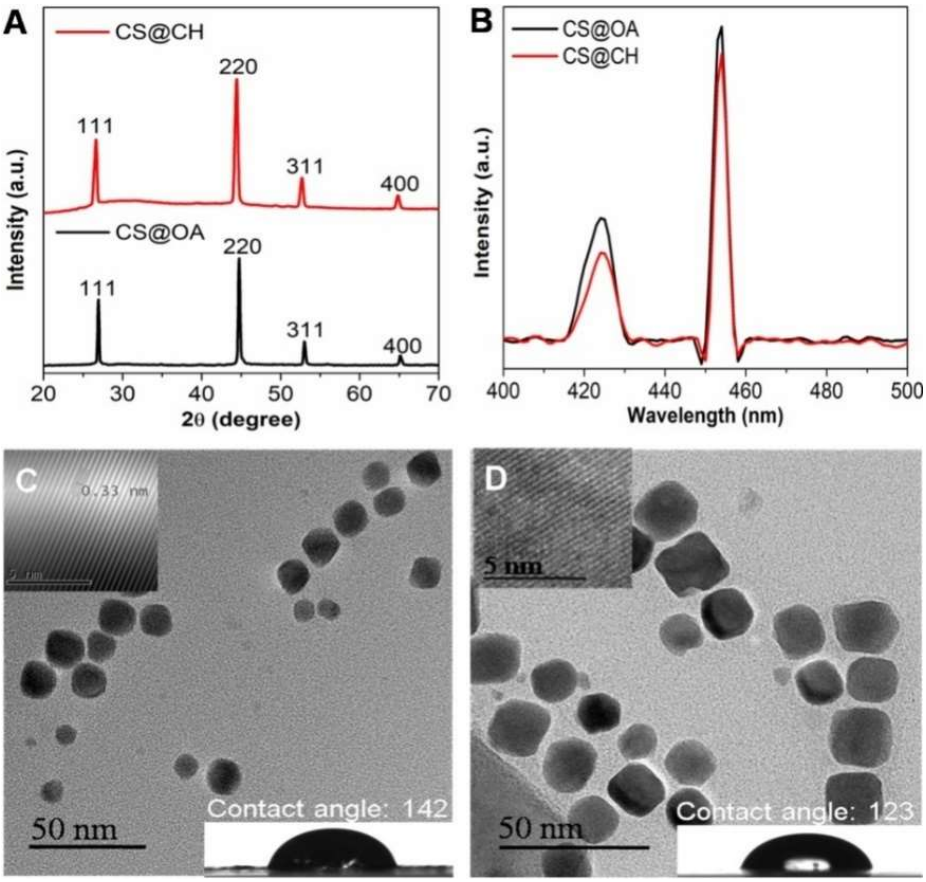

Fig. 1 Characterization of the $Cu_{2-x}Se$ NPs (as-prepared oleylamine-coated CS@OA and chitosan-coated CS@CH). (A) XRD patterns of CS@OA (black curve) and CS@CH NPs (red curve). (B) PL spectra of CS@OA (black curve) and CS@CH (red curve) recorded at a 370 nm excitation wavelength. (C, D) TEM images of CS@OA and CS@CH showing the $Cu_{2-x}Se$ NPs, respectively (Inset (top left corner): HR-TEM images of the CS@OA and CS@CH NPs showing a 0.33 nm lattice spacing, corresponding to the (111) plane of $Cu_{2-x}Se$) (Inset (bottom right corner): Contact angle on glass substrates coated with CS@OA or CS@CH NPs).

Uptake study

Following the material characterization, both CS@OA and CS@CH NPs were sprayed onto the roots of 30-day-old plants. One group was sprayed with CS@OA NPs, and the other group was sprayed with CS@CH NPs. After brief air drying, the plants were incubated in the hydroponic medium. The NPs that had not landed on the roots were collected on a glass backstop and estimated to be ~200 µg. The root and shoot samples were collected at 1.5, 3, 6, 12 and 24 h intervals, oven dried and then quantified with inductively coupled plasma mass spectrometry (ICP-MS) after microwave acid digestion (Fig. 2A, B). Before oven drying and digestion steps, the root biomass of samples collected after every time intervals were washed with 0.1 M HNO_3, to remove the NPs just adhered without uptake by the root [50]. The scanning electron microscope (SEM) images of the unwashed roots (Additional file 1: Fig. S5) and after washing with 0.1 M HNO_3 (Additional file 1: Fig. S6) confirms that the adhered particles were removed. The uptake study (Fig. 2A) clearly shows that the hydrophobic CS@OA NPs have the ability to quickly enter into the roots and are taken up at a rate that is ~1.3 times the uptake rate of the hydrophilic CS@CH NPs after the initial 1.5 h incubation with the root.

The uptake concentration started to decrease gradually in the root, unlike previous studies where a continuous increase in the NPs content in the root was observed. This is obviously because of the 1. lack of continuous NPs supply from the medium, unlike in previous studies, 2. transport to the shoot from the root (Fig. 2B), and 3. possible restriction of any particles adhered to the root. Despite the unavailability of additional NPs in the incubation medium, the uptake in the roots has been found to be more than that in the shoot at any given time point in the 24 h observation period. This may be due to an inhibition of the NPs movement, which is in agreement with the previously reported long observation times for different hydrophilic NPs compared to that of ions [19,51,52]. Restriction of movement across the tissue in hydrophilic CeO_2 particles resulted in their dissolution into ions after 4 days [18]. Interestingly, ratio of the NPs movement to shoots from the roots have been found higher in the treatment sprayed with hydrophilic NPs (0.72) than in the hydrophobic NPs (0.48) (Fig. 2C). We also quantified the leaching of Cu ions from CS@OA and CS@CH NPs in the medium by ICP-MS after 24 h of incubation and found ~1.5 % copper in CS@OA and < 1.5 % in CS@CH NPs, which is insignificant to influence the treatment.

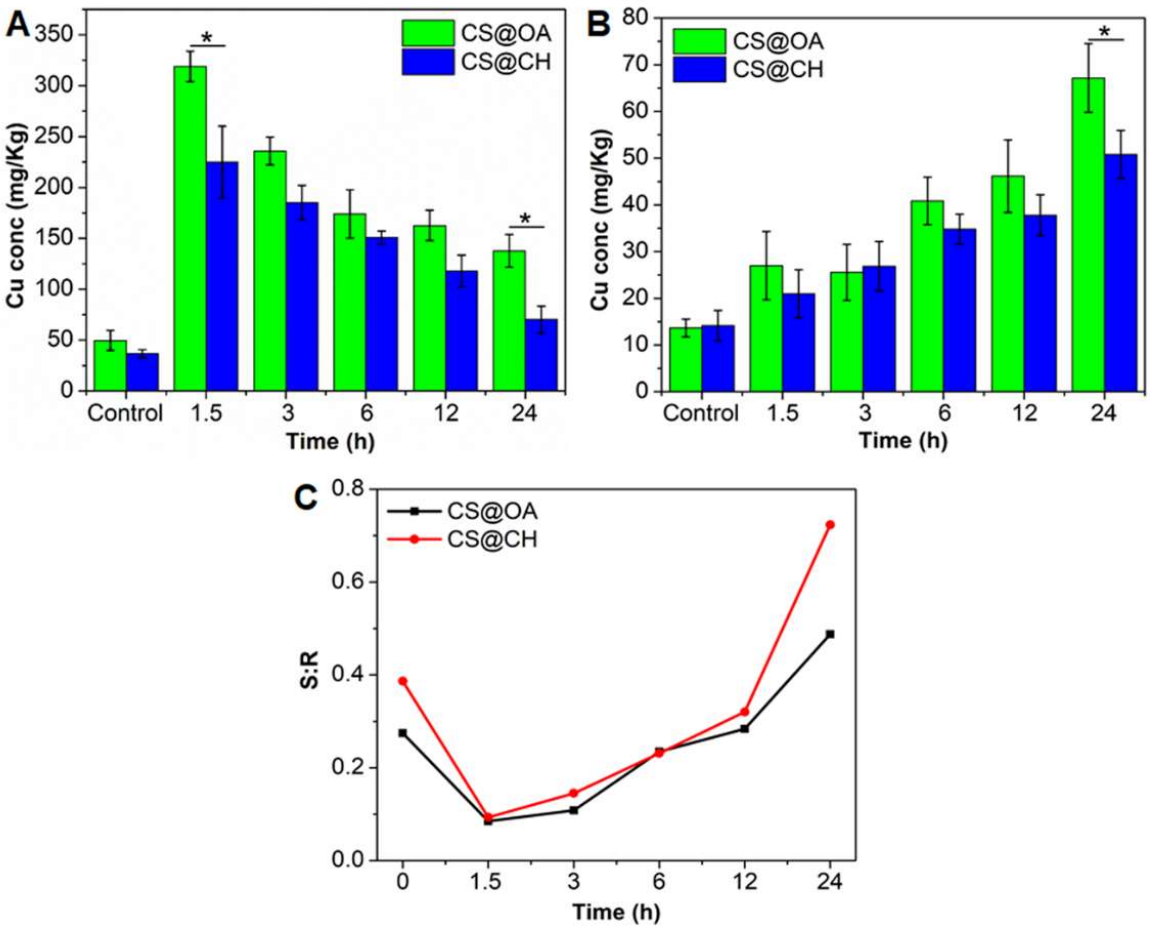

165

166 **Fig. 2** (A, B) Copper accumulation in the roots (A) and shoots (B) at different incubation times
167 after spraying the roots with either CS@OA or CS@CH NPs estimated with ICP-MS (The
168 copper concentration is normalised to per kg of root and shoot dry weight). (C) Shoot: root
169 copper content ratio.

170 The intense fluorescence from the $Cu_{2-X}Se$ NPs allowed the NPs to be tracked in the plant
171 tissue; here, an image taken from a root after 1 h of incubation using confocal laser scanning
172 microscopy (CLSM) is given in Fig. 3A-D. This study confirms that the uptake occurred as
173 intact NPs in the plant tissue rather than by dissolution or oxidation of the NPs to ions. The 3D
174 CLSM images of the tissues treated with CS@OA and CS@CH NPs are given in videos 1 and 2,
175 respectively. This was further confirmed by the TEM micrographs of the microtome sections of
176 the roots after 3 h of incubation (*vide infra*).

Following the CLSM study, the microtome sections of the roots were stained and observed by TEM. In the TEM images, the darkly contrasted CS@CH and CS@OA NPs shows differences in their patterns of particle aggregation, distribution and transport in the tissue. The hydrophobic CS@OA NPs have been predominantly present in the intercellular region and showed similarly restricted movement as that observed for the less hydrophilic pristine carbon nanotubes in plant cells; however, in that study the polarity wasn't discussed [53] (Fig. 3E). CS@OA NPs aggregation in the intercellular space may be due to cell wall lipid assisted liposome formation and may eventually restrict its intracellular movement. Within the intercellular area, a major portion of the hydrophobic CS@OA NPs have been found to be aligned in the bilayer cell membranes unexposed to the polar heads (encircled in black gradient lines). The element composition of these particles was confirmed with point EDX elemental analysis (Additional file 1: Fig. S7); the nickel signal observed is from the grid, since nickel grid was used in place of copper grid to avoid copper signal overlap and lead signal observed is from the staining agent. In the hydrophobic CS@OA NPs-treated plant, many endocytosis-like bodies have been observed (encircled in red), which once again supports lipid-covered body formation in the hydrophobic treatment. Supporting this claim, hydrophobic NPs were reported to easily form liposomes through bilayer disruption [34]. In contrast, the hydrophilic CS@CH NPs have been found predominantly distributed in the intracellular region, which may be due to the ability of the hydrophilic NPs to interact with the polar head groups of the cell membrane (Fig. 3F). However, this does not negate the possibility of CS@CH NPs movement in the intercellular region. A closer look at the gradient circle shows NPs-aligned movement without aggregation. Both CS@OA and CS@CH NPs did occupy the intercellular gas space. The predominant intracellular distribution of the CS@CH NPs and their well distributed (without aggregation) intercellular presence may be due to their compatibility with aqueous medium. Unlike hydrophobic NPs, in CS@CH NP treatment, endocytotic bodies have not been observed which may be due to their ability to directly enter the cell. Similar direct entry without endocytosis was observed in plant protoplast cells [54]. The particle size distribution in the intercellular space is given in Additional file 1: Fig. S8 (the microtome location of the NPs is given just above the graph), which confirms the stability of the NPs in the plant tissue. However, over time, they may not be stable due to the enzymatic action of the plant, especially in the leaves, and over time, the particles may dissociate into ions, as previously observed by radioactive signals [18].

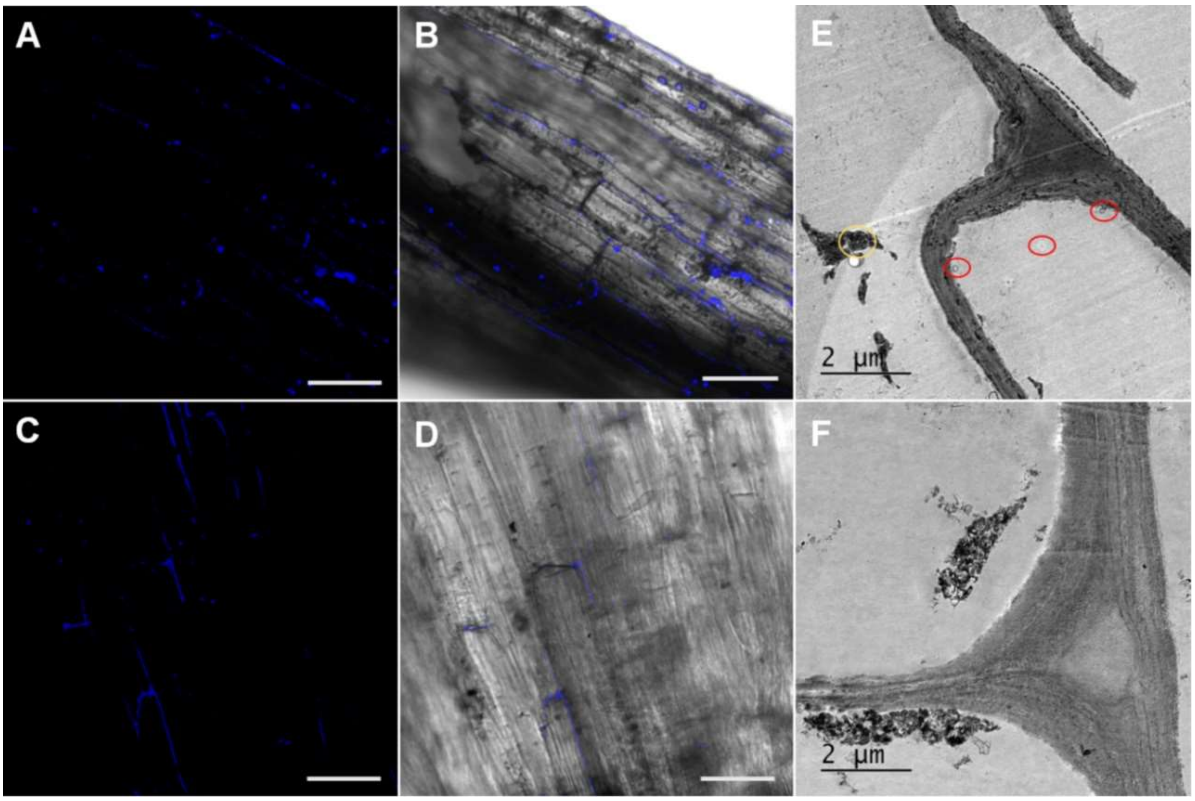

Fig. 3 Confocal and TEM images of tomato plant tissue showing NPs uptake. (A-D) show the confocal images of tomato roots sprayed with CS@OA (A, B) and CS@CH (C, D) NPs after 1 h of incubation time merged with the brightfield image (scale bar is 20 µM). (E, F) TEM images of the microtome sections of tomato roots sprayed with CS@OA (E) and CS@CH (F) after 3 h of incubation time.

Mechanism of uptake

AFM adhesion force measurements

The enhanced penetration of CS@OA NPs into the root may be due to their binding, which motivated us to measure the force *vs.* distance between the root and the NPs in water using AFM. AFM silicon nitride tips were modified with CS@OA and CS@CH, separately, by incubation in the respective solutions for 5 h followed by sequential washing with water and ethanol. A fresh root tip was fixed onto a glass plate with a resin that could dry fast without any cross reactions in order to keep the root alive [29,55,56]. Following this, water was added carefully with a syringe, and the AFM tip was placed in contact with the root with the assistance of the microscope. The maximum from the Gaussian fitting of the adhesion force experienced by the CS@OA NPs has

been found to be ~500 pN more than the force experienced by the CS@CH NPs (Fig. 4A, B). This adhesion could be driven by 3 reasons: 1. water, which pushes the hydrophobic NPs towards a solid substrate (here the root) or the hydrophobic particles unwillingness to allow water into the root/particle interspaces, 2. manipulation of the contacted hydrophobic NPs surface to become sticky with the ions present on the root surface [34], and 3. as mentioned above, the ability of the hydrophobic NPs to penetrate the lipid surface [34]. Thus, active uptake where the energy contribution comes from the NPs, unlike classical active transport where the energy is expended by the plants, is identified. Thus, the adhesion force expressed by the NPs corroborates to the root uptake proportionally, similar proportional uptake was also reported earlier in the animal cells [57]. The maximum adhesion force expressed by the hydrophobic NPs have led to the enhanced root uptake.

Protein corona study

The curiosity to understand the ability of the hydrophilic NPs to show a greater root to shoot transport ratio motivated us to study its protein corona in comparison to that of the hydrophobic NPs. Protein coronae, which changes with the surface often decide the fate of NPs in animals [58–60]; which has been ignored in plants, is studied here by 2D- polyacrylamide gel electrophoresis (PAGE). The intact NPs from the plant tissues were obtained by enzyme-assisted extraction following the protocol standardized by Dan et al [15]. In 2D gels, protein spots have been found to be distributed within a molecular mass range of 19-43 kDa and covering the pH range of 4.3-9.6. For the CS@OA NPs, 10 protein spots have been detected, while 14 protein spots have been detected for the CS@CH NPs. In the CS@OA sample, 2 proteins have been found down-regulated (numbers 4 and 10), and 4 protein spots have not been detected (numbers 11, 12, 13 and 14) compared to the proteins detected in the CS@CH sample (Fig. 4C, D). Interestingly, all of these protein spots (except 13) have been observed at acidic pH. To explain this pattern, close approximations of foreign body movements in roots *viz*., a mycorrhizal association report were compared. A similar downregulation of an acidic pI membrane protein was observed in tomato by mycorrhizal association [61], which may be the adaptation strategy of the plant to restrict them in the root zone. Additionally, the presence of a few spots in the higher pI range for the CS@OA sample are poorly separated due to the poor protein solubility and contaminants in the buffer, which interfered with staining. Therefore, they may not be considered protein spots.

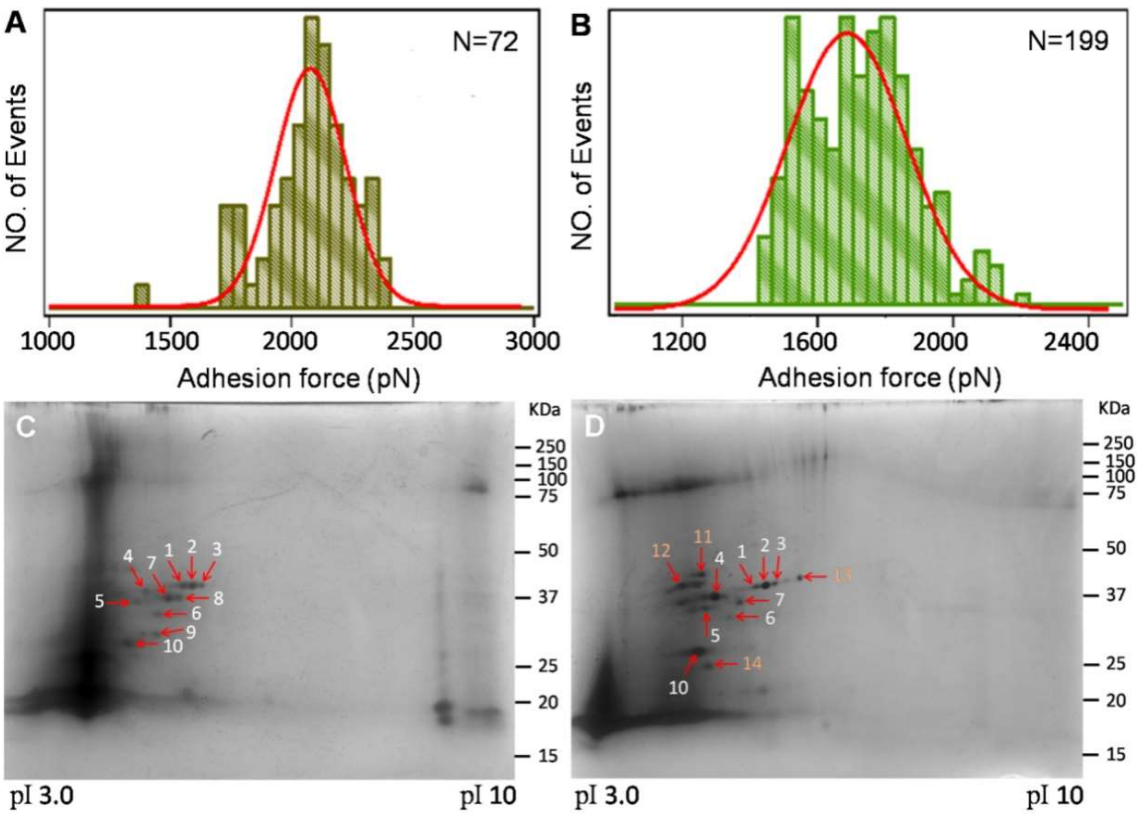

Fig. 4 (A, B) Adhesion force between the root and an AFM tip modified with either CS@OA (A) or CS@CH (B) NPs in water. (C, D) 2D gel pattern of the protein corona extracted from roots with CS@OA (C) and CS@CH NPs (D) in a pH gradient of 3-10 with silver staining.

Toxicity study

Finally, after elucidating the uptake mechanism, the toxicities of the hydrophobic and hydrophilic NPs were compared by using the ascorbate peroxidase (APOX) and catalase (CAT) activity assays. In roots, the APOX activity has been found to be increase after incubation with the NPs, especially at 1.5 h (Fig. 5A). The initial stress due to the plant uptake of foreign bodies may have resulted in the synthesis of H_2O_2, whose enzymatic conversion may have raised the APOX activity [50]. Interestingly, with increasing incubation time, the activity has been found to be reduced, possibly because the plant adapted to the initial NPs load and because there is no further accumulation. In the shoots, the APOX activity has been found to be increase after 12 h of incubation, which may have been due to the time needed for a threshold amount of NPs accumulation to trigger APOX in the shoot (Fig. 5B). In case of the CAT activity, the reduction in the activity has been noted (Fig. 5C, D), which is contrary to the previous studies on metal

NPs uptake [62]. There are few studies where reduction in the CAT activity was also documented in the presence of an overexpression of the APOX activity, for instance here APOX is overexpressed, which can control oxidative stress [50,63]. Visual observation of the plants over 3 days surprisingly shows that the plants incubated after being sprayed with CS@OA NPs found to healthier than the plants incubated after being sprayed with CS@CH NPs. Further, the MTT assay was also performed to evaluate the toxicity caused by the CS@OA and CS@CH NPs. The assay shows the biocompatibility of the NPs because the percent root viability has been found to be >90 % after 24 h of treatment with CS@OA and CS@CH NPs (Additional file 1: Fig. S9). Thus, at a 100 µg/plant concentration, no visual effect on plants incubated with hydrophobic NPs. Apart from the NPs concentration; there is a fair chance that trace amounts of selenium ions could have leached from the particles and enhanced the antioxidant/photosynthetic activity and photo-oxidative stress control [64–68].

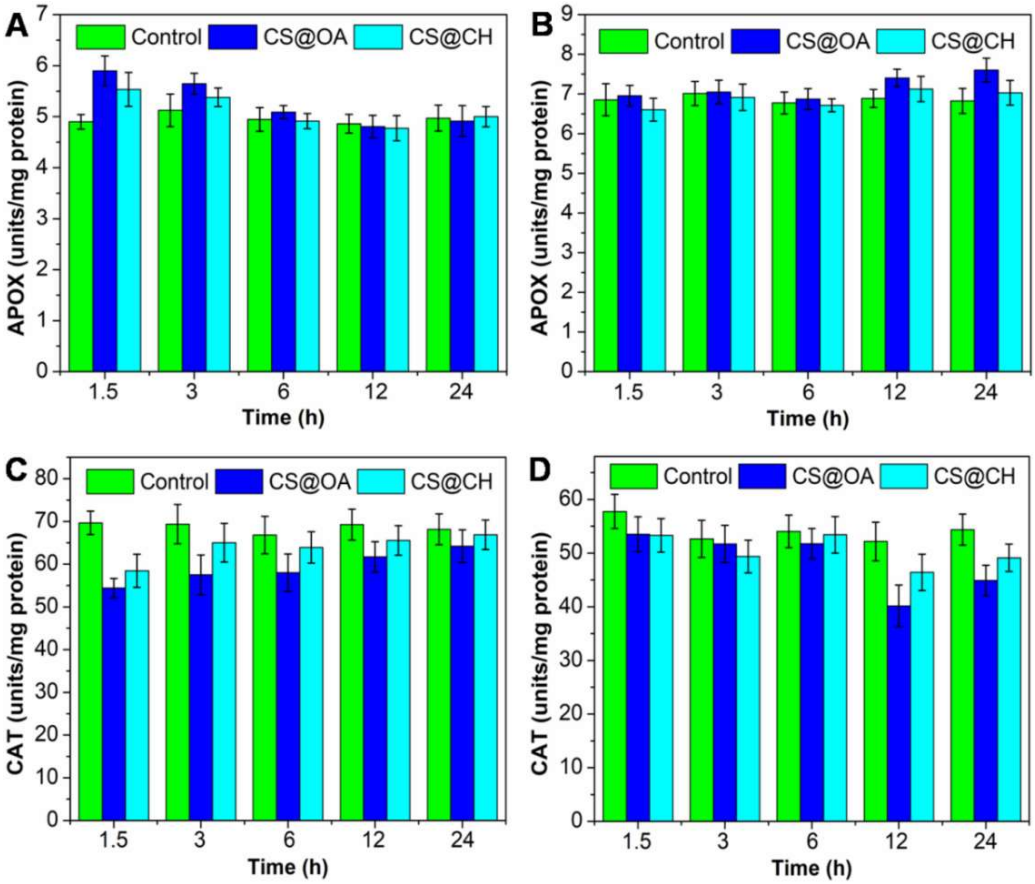

Fig 5. APOX and CAT antioxidant activity in tomato roots (A, C) and shoots (B, D) after exposure to $Cu_{2-x}Se$ (CS@OA and CS@CH) NPs compared to the control plants at different time points.

Conclusions

Previous experience regarding NPs uptake has confirmed that uptake is genus, species, variety, material, age, concentration and size dependent. However, there were no reports on the effects of NPs with hydrophobic surfaces, which are explained here. The enhanced uptake of hydrophobic NPs by the roots proves that non-classical forced penetration is more efficient. Hence, this enhanced uptake and sedentary behavior of hydrophobic NPs in root can be adopted for eco-friendly leach-proof fertilizer application. This report also serves as an early warning to avoid exposing undesired hydrophobic NPs to edible plants in the context of enhanced phytoaccumulation. Furthermore, TEM images taken at early incubation period reveal a predominance of hydrophobic NPs in the membrane bilayer, which has the future potential for spatial targeting in plants.

Methods

Materials

Ethanol, methanol, chloroform, glacial acetic acid, HNO_3, H_2O_2, Na_2HPO_4, NaH_2PO_4, $AgNO_3$, Na_2CO_3 and sodium dodecyl sulphate (SDS) were purchased from Merck, Bengaluru, India. Bovine serum albumin and chitosan powder were purchased from Sisco Research Laboratories, Chandigarh, India. Glutaraldehyde was purchased from TCI chemicals, Chandigarh, India. A Spurr resin kit and OsO_4 were purchased from Electron Microscopy Sciences, Delhi, India. Uranyl acetate was purchased from LobaChemie, India. CuCl, selenourea, oleylamine, citric acid, sodium citrate monobasic, lead citrate, Laemmli buffer, ammonium persulfate, Trizma base, tetramethylethylenediamine (TEMED), acrylamide, *N,N′*- methylenebis(acrylamide), 3-(4,5-dimethythiazol-2-yl)-2,5-diphenyl tetrazolium bromide (MTT), KOH, phenylmethylsulfonyl fluoride (PMSF) cocktail, KH_2PO_4, K_2HPO_4, glycerol and formaldehyde were purchased from Sigma-Aldrich, Bengaluru, India. Bradford reagent, macerozyme R-10, 1× phosphate buffer saline (PBS), sodium thiosulfate and ascorbate were purchased from HiMedia, Mumbai, India. Rehydration buffer, IPG strips of pH range 3–10, a ReadyPrep 2D starter kit equilibration buffer I and II and a ReadyPrep™ 2D clean-up kit were purchased from Bio-Rad, Gurugram, India. A precision plus protein™ kaleidoscope™ prestained protein ladder was purchased from Bio-Rad.

Synthesis of $Cu_{2-x}Se$ NPs (CS@OA)

The arrested precipitation method was adopted for the synthesis of $Cu_{2-x}Se$ NPs with minor modifications [69]. In brief, a nitrogen-filled glove box (< 0.5 ppm oxygen) was employed for the preparation of the precursor mixtures. First, copper and selenium reactant mixtures were individually prepared and allowed to react simultaneously by hot injection. The copper reactant was prepared by the addition of 10 mL of oleylamine to 0.198 g of cuprous chloride in a round-bottom flask. Then, the mixture was heated under nitrogen environment to 130 °C for 15 minutes along with stirring using stir bar. The solution was cooled to 100 °C before injection of selenium. The selenium reactant was prepared by the addition of 1 mL of oleylamine to 0.123 g of selenourea in a round-bottom flask. Then, the mixture was heated under nitrogen conditions to 200 °C for 10 minutes with stirring. Selenourea and oleylamine were injected into a flask containing cuprous chloride and oleylamine after being cooled to 160 °C. After injection, the solution appeared black and was further heated to 240 °C for half an hour. Then, the solution was allowed to cool to room temperature. The synthesized CS@OA NPs were precipitated by adding 10 mL of ethanol and washed 5 times with a chloroform-ethanol mixture with a ratio of 1:2 and finally dried under reduced pressure of 65 cm Hg.

Synthesis of chitosan-coated $Cu_{2-x}Se$ NPs (CS@CH)

The synthesized CS@OA NPs powder (10 mg) was dispersed in 10 mL of a chitosan solution by bath sonication for 30 minutes. The chitosan solution was prepared by adding 50 mg of chitosan powder to 10 mL of distilled water at pH 4.5 under stirring. The pH of the distilled water was adjusted by glacial acetic acid [70]. After dispersion, the solution was centrifuged at 12,000 rpm for 10 minutes to remove unbound free polymer, followed by washing with distilled water. Finally, the chitosan-coated CS@OA NPs were dispersed in distilled water.

Characterization of CS@OA and CS@CH NPs

A Bruker D8 Advance diffractometer with a Cu $K\alpha_1$ radiation source (λ = 1.5406 Å) was used for XRD pattern analysis at 40 kV and 25 mA. A Cary 600 series FT-IR spectrophotometer (Agilent Technologies) was used to record the FT-IR spectra. The contact angle was measured by DIGIDROP modular contact angle technology and analysed by Visio drop software. For this study, CS@OA and CS@CH NP samples were dispersed in ethanol and distilled water, respectively, and a film was prepared by coating the samples onto a glass substrate surface. The

glass substrate and other surfaces were cleaned with acetone and ethanol using a cotton swab, dried with a clean cotton swab and then placed onto the sample stage. The contact angle was measured by gently depositing a drop of deionized water onto the film on the substrate surface using a microsyringe at ambient temperature. The contact angle was measured instantly after contact of the water drop with the NP film. Contact angle was calculated by the computer software in the goniometer without the operator intervention. UV-visible absorption spectra were recorded by a UV-visible spectrophotometer (UV-2600, Shimadzu). An Edinburgh instrument was used to record the PL emission spectra at 370 nm excitation wavelength. For UV-Visible and PL analysis, CS@OA and CS@CH powders were dispersed in an ethanol-water mixture with a ratio of 1:1 at a concentration of 300 ppm. A JEOL JEM-2100 microscope was used for TEM and HR-TEM analysis at 200 kV. The samples were prepared by dropping 7 μL of a highly diluted and dispersed sample solution onto a carbon-coated copper grid and wicking off excess solution after 1 minute with filter paper. The size distribution on TEM images was calculated by using Image-J software. A Malvern Zetasizer Nano ZSP instrument was used to measure the hydrodynamic diameter of each sample at 25 °C. Well-dispersed samples of 50 ppm concentration was prepared for the hydrodynamic diameter measurements were added into a clear glass Dynamic light scattering (DLS) cuvette. In parameters, total three runs were set for each sample, each run was for 2 minutes and the equilibration time was set 120 seconds.

Instrumentation in determining NPs and plant interaction

The copper concentrations in root tissues were quantified by using ICP-MS (Agilent 7700 series). CLSM (Carl Zeiss microscope LSM 800) was used to locate the CS@OA and CS@CH NPs in the root cells. CLSM images were processed using ImageJ software. AFM experiments were carried out on a commercial AFM instrument (Force Robot 00574, JPK Instruments, Berlin, Germany). The force-distance curves were recorded by commercial software from JPK and analysed by custom-written procedures in Igor pro 6.2 (Wavemetrics, Inc.). For the experiment, CS@OA and CS@CH NPs were dispersed in ethanol and water, respectively, at a concentration of 300 ppm. The PROTEAN® i12™ IEF system (Bio-Rad) was used for the separation of proteins in the first dimension, and the Mini-PROTEAN® system (Bio-Rad) was used for the separation of proteins in the second dimension. Gel pictures were captured by using Gel Doc (Bio-Rad) with Image Lab software.

Uptake study of CS@OA and CS@CH NPs

Plant treatment. As characterised particles were applied aeroponically on the tomato roots following the standard procedure [71,72]. For this study, 30-day-old tomato plants were collected from the green house and sorted in such a way that they have approximately similar biometric parameters (9-10 cm, and the root lengths were 1.5-2 cm) and divided into 2 groups. The as-prepared hydrophobic CS@OA NPs were dispersed in ethanol, and the hydrophilic CS@CH NPs were dispersed in distilled water for spraying. One group of plants was sprayed with the CS@OA NPs, and the other group was sprayed with CS@CH NPs, dispersed in 1 mL respective solvent at 300 ppm concentration. After briefly air drying, the plants were incubated in the 20 mL hydroponic medium for 1.5, 3, 6, 12 and 24 h, following which the samples were oven dried and then quantified with ICP-MS after microwave acid digestion. The NPs that had not landed on the roots were collected on a glass backstop from two samples per treatment, digested and analyzed with the ICP-MS. Details of the ICP-MS protocol is given below.

ICP-MS analysis. After the specified time period, the plants were collected and washed with 0.01 M HNO_3 and Milli-Q water to remove any adhered particles that had not entered the roots. Then, the plants were sectioned into roots and stems (cut 5 cm from the shoot start point) and dried properly at 60 °C in an oven and weighed. The dry weights of the 50 mg roots and 150 mg shoots were taken for the metal content analysis. The treated samples were then digested by using 1 mL of metal-grade HNO_3 and H_2O_2 (1:4) as described previously [50]. Then, the samples were diluted 13-fold in distilled water and analysed using ICP-MS.

Further, to quantify the leaching of copper ions from CS@OA or CS@CH NPs, the medium in which the plant was sprayed and incubated for 24 h, was collected. This medium was centrifuged at 10,000 rpm for 30 minutes to evaluate the supernatant ion concentration with ICP-MS.

CLSM analysis. For this experiment, the plant root tissue was treated with a 1 mL solution of CS@OA or CS@CH NPs at a concentration of 300 ppm by using a sprayer. After 1 h, the root tissue was excised from the treated plant and washed thoroughly with deionized water. Then, the root tissue was placed in an FAA fixative solution containing 37 % formaldehyde (v/v), 5 % glacial acetic acid (v/v), 45 % ethanol (v/v) and 45 % distilled water (v/v), followed by vacuum infiltration for 15 minutes. After that, the root tissue was transferred

into a fresh FAA fixative solution overnight at 4 °C. Then, the root samples were washed three times with phosphate buffer for 10 minutes each. Tissues were then dehydrated through a 30, 50, 75, 90 and 100 % graded series of ethanol for 15 minutes each. Prior to microscopy, sample clearance was performed to increase the tissue transparency. For this, tissues were passed through 25, 50, 75 and 100 % concentrations of glycerol for 1 h each with two changes of each solution and then incubated overnight in pure glycerol [73]. Cleared tissues were then mounted on long cover slips in glycerol and covered by small cover slips. Images were acquired by CLSM in the blue region after excitation at 405 nm, and emission was collected in the wavelength range of 410-480 nm.

Root tissue section preparation for TEM imaging. For this study, the plant roots were treated with 1 mL of a CS@OA or CS@CH NP solution at a concentration of 300 ppm by using a sprayer. After 3 h, the roots were excised from the treated plants and washed thoroughly with deionized water. Then, the root samples were fixed with a 5 % glutaraldehyde solution followed by incubation for 2 h at 4 °C. Then, the root samples were washed three times with phosphate-buffered saline for 10 minutes each time. After that, several steps, such as osmication with 1 % osmium tetroxide, *En bloc* staining with 2 % uranyl acetate and dehydration with a graded series of ethanol followed by infiltration with embedding medium, were performed as reported [74]. Then, a few drops of the Spurr resin were placed into moulds, followed by transfer of the root samples into the moulds. The remaining space in the moulds was filled with Spurr resin, and then the moulds were kept overnight at 60 °C for polymerization. Then, the samples were sectioned into 70-80 nm thick samples with a Leica EM UC6 ultra-microtome, followed by staining with uranyl acetate and lead citrate. The root tissue sections were then placed on nickel grids and analysed by TEM.

Uptake mechanism of CS@OA and CS@CH NPs

AFM force measurements. The forced was measured by modifying AFM silicon nitride tips with CS@OA and CS@CH NPs and fixation of fresh root tip onto a glass plate by using epoxy resin [30,55,56]. First, the glass cover slips were placed in a warm chromium acid solution for 3 h to remove residual organic matter and then rinsed with Milli-Q water followed by drying under a stream of nitrogen. AFM silicon nitride tips were modified with CS@OA and CS@CH separately, by incubation in the respective solutions for 5 h followed by sequential washing with

water and ethanol. A fresh root tip was fixed onto a glass plate with an epoxy resin that could dry fast without any cross reactions in order to keep the root alive. Following this, water was added carefully with a syringe, and the AFM tip was placed in contact with the root with the assistance of the microscope and the adhesion force was measured. The protocol we selected was to record single measurements at different points along the length of the root by taking several measurements at the root surface. AFM silicon nitride cantilevers with silicon nitride tips (type MLCT, from APP NANO) were used in all of the experiments. The spring constants of the tips were calibrated by the thermal fluctuation method and were all in the range of 0.040-0.075 N m^{-1}. All of the experiments were carried out at a pulling speed of 1000 nm sec^{-1}. The AFM experiments were conducted after allowing the system to equilibrate for 30 minutes. All of the AFM force measurements were carried out at 25 ± 1 °C.

Protein corona study. For this study, 30-day-old plants of the same length and weight were used for each treatment. Afterwards, the plant roots were treated with 1 mL of CS@OA or CS@CH NP solutions at a concentration of 300 ppm by using a sprayer, and the plants were then transferred into hydroponic medium for 3 h. Then, two grams of root from all the treated plants were collected and ground in liquid nitrogen with a mortar and pestle. Then, the ground tissue powder from each treatment was added to 10 mL of a 2 mM citrate buffer at pH 4.5, followed by homogenization of the samples in an ice bath. Then, a 0.5 mM phenylmethylsulphonyl fluoride (PMSF) cocktail was added to each treatment solution to inhibit protease. The optimum pH range should be 3.5–7.0 for activity of the macerozyme R-10 as provided by the manufacturer; as such, the pH of the citrate buffer was adjusted to 4.5 with citric acid. Then, 2 mL of citrate buffer containing 800 mg of the macerozyme R-10 was added to the above solution, and the samples were incubated for 24 h at 37 °C prior to being digested as reported [16]. After digestion, samples were filtered through 0.45 µm filter paper, and the filtrate was collected. Then, the samples were centrifuged at 12,000 rpm for 30 minutes at 4 °C to separate the NPs from unbound proteins. The obtained pellet for each treatment was washed several times by dispersing in 1.5 mL of 1× PBS, followed by centrifugation to completely remove NPs from the unbound proteins [75]. All of the pellets (having NPs with bound proteins) had 100 µL of a 10 % sodium dodecyl sulphate solution added to them and were kept at 95 °C in a water bath for 10 minutes, followed by centrifugation at 12,000 rpm. Then, the supernatant was collected, which had NP-

494 free protein. After that, samples were cleaned by using a ReadyPrep™ 2D clean-up kit. Finally,
495 the clean protein pellets for each treatment were used for 2D-PAGE documentation.
496 The cleaned sample pellets for each treatment were dispersed in 200 µL of rehydration
497 buffer. The entire 200 µL volume of the IPG gel rehydration buffer-containing protein samples
498 were loaded onto a 7-cm long IPG strip with a pH range of 3–10, which allows the proteins to
499 enter the IPG strip gel after an overnight rehydration and equilibration process. After that, the
500 IPG strips were transferred to an isoelectric focusing tray, and the proteins were separated by
501 using an isoelectric focusing electrophoresis unit. The IPG strips were run for a total of 10 kVh.
502 After isoelectric focusing, the IPG strips were equilibrated in equilibration buffer-I and
503 equilibration buffer-II for 10 minutes each. The equilibrated IPG strips were then used for a
504 second dimension of electrophoresis. The proteins were separated by using a 12 %
505 polyacrylamide gel. Gel electrophoresis was carried out at 100 V for approximately 80 minutes
506 until the proteins had separated to the end of the gel. Precision plus protein™ kaleidoscope™
507 prestained protein standard was used as a molecular weight marker. The gels were stained by
508 silver staining, and images were captured by a Gel Doc and analysed by the PDQuest software
509 (Bio-Rad).
510 After electrophoresis, gels were fixed in a methanol (50 mL), acetic acid (12 mL),
511 formaldehyde (50 µL) and MQ water (38 mL) mixture for 30 minutes followed by washing in a
512 methanol (20 mL) and water (80 mL) mixture for 10 minutes. Then, the gels were sensitized in
513 an aqueous solution of sodium thiosulfate (prepared by adding 20 mg to 100 mL of MQ water)
514 for 10 minutes followed by washing of the gels with excess MQ water. After that, the gels were
515 stained with a chilled silver nitrate solution (prepared by adding 200 mg of silver nitrate and 76
516 µL of formaldehyde into 100 mL of MQ water) at 4 °C followed by washing of the gels with
517 excess MQ water. Then, the gels were developed in a development solution (sodium thiosulfate
518 (0.4 mg), sodium carbonate (6 g) and formaldehyde (50 µL) in 100 mL of MQ water) under a
519 white light transilluminator. After the protein spots appeared, the development solution was
520 replaced with the stop solution (10 mL acetic acid in 90 mL distilled water) to avoid excessive
521 development.

522 **Toxicity study**

523 The toxicity of the hydrophobic and hydrophilic NPs was compared by using the ascorbate
524 peroxidase (APOX) and catalase (CAT) assays as reported [50]. For this study, the tomato roots

were treated with 1 mL of CS@OA or CS@CH NPs at a concentration of 300 ppm by using a sprayer as described above. For CAT activity, treated root and shoot tissues were excised after a specific time period and ground in liquid nitrogen with a mortar and pestle followed by homogenization in 1 mL of pH 7.4 ice-cold potassium phosphate buffer. Then, the tissue extracts were centrifuged at 4 °C for 5 minutes at 10,000 rpm, and the supernatant was collected. Then, 10 µL of the supernatant was added to 990 µL of 10 mM H_2O_2 in a quartz cuvette and mixed. The CAT activity was determined by a UV-Vis spectrophotometer based on the decrease in the reaction mixture absorbance at 240 nm over one minute.

For APOX activity, plant samples were prepared as described above. A 100 µL volume of the supernatant was added to a 1 mL quartz cuvette with 886 µL of 0.1 M potassium phosphate buffer at pH 7.4, 4 µL of 25 mM ascorbate and 10 µL of 17 mM H_2O_2 and then mixed. The APOX activity was determined with a UV-Vis spectrophotometer by measuring the decrease in the reaction mixture absorbance at 265 nm over one minute. The protein concentrations for both assays were quantified by the Bradford method using a bovine serum albumin standard curve.

Further, the root viability was studied by MTT assay as reported [76]. In brief, the plant roots were treated with 1 mL of CS@OA or CS@CH NPs as described above and incubated for 24 h. After that, 10 mg of the fresh root tissue was taken and transferred to the 2 mL centrifuge tube followed by the addition of MTT dye. After 4 h of incubation in the dark, the MTT solution was discarded and the root tissues were transferred to the fresh petriplates. The root tissue was cut with sterile scalpel into 1-2 mm pieces followed by the addition of 0.5 mL of KOH solution to this. The cut root pieces along with the KOH solution was transferred to the 2 mL of centrifuge tubes and 0.5 mL of DMSO solution was added to each tube to make the total volume of 1 mL. Then, the tubes were centrifuged at room temperature at 500×g for 5 minutes. The supernatant was transferred to fresh tubes, resultant absorbance was measured at 570 nm and cell viability was calculated.

Statistical analysis

GraphPad Prism 8.0 software was used for all the statistical data analyses. All data were plotted as mean ± standard error. Nonparametric t-test was used to reveal the significant difference at 95 % confidence level ($P < 0.05$), as denoted by *asterisks. The data not showing asterisks, reveal not significant.

Supplementary information

Supplementary information accompanies this paper at https…

Additional file 1: Figure S1. FT-IR spectra of CS@OA and CS@CH NPs. **Figure S2.** Fluorescent images of; (A) dispersion of CS@OA NPs in ethanol, (B) aggregation of hydrophobic CS@OA NPs in distilled water, (C) dispersion of CS@CH NPs in distilled water. **Figure S3.** UV-Visible spectra of CS@OA and CS@CH in 1:1 ratio of ethanol/water mixture. **Figure S4.** DLS of CS@OA and CS@CH NPs. **Figure S5.** SEM image of the roots not washed with 0.1M HNO_3 after incubation with (A) CS@OA and (B) CS@CH NPs. **Figure S6.** SEM image of; (A, B) Root washed with 0.1M HNO_3 after incubation with CS@OA and (C, D) CS@CH NPs (Images are capture at two different area and different scale bar of 10 μm, 2 μm and 500 nm). **Figure S7.** Point EDX performed on various NPs showing the signal for copper. **Figure S8.** Particle size distribution of CS@OA and CS@CH NPs in plant root tissue. **Figure S9.** The MTT assay showing the root viability after 24 h of treatment with CS@OA and CS@CH NPs.

Abbreviations

AFM: Atomic force microscope; CLSM: Confocal laser scanning microscopy; DLS: Dynamic light scattering; FT-IR: Fourier transform infrared; ICP-MS: Inductively coupled plasma mass spectrometry; MTT: 3-(4,5-dimethythiazol-2-yl)-2,5-diphenyl tetrazolium bromide; PAGE: Polyacrylamide gel electrophoresis; PBS: Phosphate buffer saline; PL: Photoluminescence; PMSF: phenylmethylsulfonyl fluoride; SDS: Sodium dodecyl sulphate; SEM: Scanning electron microscope; TEM: Transmission electron microscope; TEMED: tetramethylethylenediamine; XRD: X-ray diffraction.

Declarations

Acknowledgements

The authors thank Prof. Pijush Ghosh from IIT Chennai, for readily granting access to contact angle measurement; Dr. Vikas Rishi and his technician Mr. Atul form NABI, Mohali for ICP-MS measurement.

Authors' contributions

Dr. Vijayakumar Shanmugham conceived the idea, supervised the experiments and wrote the paper. Sandeep Sharma performed the experiments, analyzed the data and assisted with the writing of the paper. Dr. Saraladevi Muthusamy performed the 2D-PAGE analysis and Dr. Selvaraju Kanagarajan assisted in writing the 2D-PAGE results, editing and commented on the manuscript. Pardeep Kumar Vaishnav prepared the root sections for TEM imaging. Dr. Manish Singh performed the TEM imaging. Dr. Deepak Sharma and his student Dr. Mohd. Muddassir performed AFM experiments and processed the AFM data.

Funding

P. S.V. is thankful to DST Nano mission, Government of India (SR/NM/NS-1434/2014(G)), for financial aid.

Availability of data and materials

All data generated or analyzed during this study are included in this published article [and its Additional file 1].

Ethics approval and consent to participate

Not applicable.

Consent for publication

Not applicable.

Competing interests

The authors declare that they have no competing interests.

References

1. Beachy R, Bennetzen JL, Chassy BM, Chrispeels M, Chory J, Ecker JR, et al. Divergent perspectives on GM food. Nat Biotechnol. Nature Publishing Group; 2002;20:1195–6.

2. Wang H, Zhang M, Song Y, Li H, Huang H, Shao M, et al. Carbon dots promote the growth and photosynthesis of mung bean sprouts. Carbon. Elsevier Ltd; 2018;136:94–102.

3. Giraldo JP, Landry MP, Faltermeier SM, McNicholas TP, Iverson NM, Boghossian AA, et al. Plant nanobionics approach to augment photosynthesis and biochemical sensing. Nat Mater. Nature Publishing Group; 2014;13:400–8.

612 4. Sonkar SK, Roy M, Babar DG, Sarkar S. Water soluble carbon nano-onions from wood wool
613 as growth promoters for gram plants. Nanoscale. Royal Society of Chemistry; 2012;4:7670–5.
614 5. Khodakovskaya M V., De Silva K, Nedosekin DA, Dervishi E, Biris AS, Shashkov E V., et al.
615 Complex genetic, photothermal, and photoacoustic analysis of nanoparticle-plant interactions.
616 Proc Natl Acad Sci U S A. National Academy of Sciences; 2011;108:1028–33.
617 6. Yin J, Wang Y, Gilbertson LM. Opportunities to advance sustainable design of nano-enabled
618 agriculture identified through a literature review. Environ. Sci. Nano. Royal Society of
619 Chemistry; 2018. p. 11–26.
620 7. Zhao P, Yuan W, Xu C, Li F, Cao L, Huang Q. Enhancement of Spirotetramat Transfer in
621 Cucumber Plant Using Mesoporous Silica Nanoparticles as Carriers. J Agric Food Chem.
622 American Chemical Society; 2018;66:11592–600.
623 8. Zhao P, Cao L, Ma D, Zhou Z, Huang Q, Pan C. Translocation, distribution and degradation
624 of prochloraz-loaded mesoporous silica nanoparticles in cucumber plants. Nanoscale. Royal
625 Society of Chemistry; 2018;10:1798–806.
626 9. Camara MC, Campos EVR, Monteiro RA, Do Espirito Santo Pereira A, De Freitas Proença
627 PL, Fraceto LF. Development of stimuli-responsive nano-based pesticides: Emerging
628 opportunities for agriculture. J. Nanobiotechnology. BioMed Central Ltd.; 2019. p. 1–19.
629 10. Le VN, Rui Y, Gui X, Li X, Liu S, Han Y. Uptake, transport, distribution and Bio-effects of
630 SiO2 nanoparticles in Bt-transgenic cotton. J Nanobiotechnology. BioMed Central Ltd.; 2014
631 ;12:50.
632 11. Wang Y, Chang CH, Ji Z, Bouchard DC, Nisbet RM, Schimel JP, et al. Agglomeration
633 Determines Effects of Carbonaceous Nanomaterials on Soybean Nodulation, Dinitrogen Fixation
634 Potential, and Growth in Soil. ACS Nano. American Chemical Society; 2017;11:5753–65.
635 12. Hu J, Guo H, Li J, Wang Y, Xiao L, Xing B. Interaction of γ-Fe2O3 nanoparticles with
636 Citrus maxima leaves and the corresponding physiological effects via foliar application. J
637 Nanobiotechnology. BioMed Central Ltd.; 2017;15:51.
638 13. Zhao J, Ren W, Dai Y, Liu L, Wang Z, Yu X, et al. Uptake, Distribution, and Transformation
639 of CuO NPs in a Floating Plant Eichhornia crassipes and Related Stomatal Responses. Environ
640 Sci Technol. American Chemical Society; 2017;51:7686–95.
641 14. Marshall CE, Upchurch WJ. Free Energy in Cation Interchange as Illustrated by Plant Root–
642 Substrate Relationships. J Phys Chem. American Chemical Society; 1953;57:618–21.

15. Dan Y, Zhang W, Xue R, Ma X, Stephan C, Shi H. Characterization of Gold Nanoparticle Uptake by Tomato Plants Using Enzymatic Extraction Followed by Single-Particle Inductively Coupled Plasma–Mass Spectrometry Analysis. Environ Sci Technol. American Chemical Society; 2015;49:3007–14.

16. Jiménez-Lamana J, Wojcieszek J, Jakubiak M, Asztemborska M, Szpunar J. Single particle ICP-MS characterization of platinum nanoparticles uptake and bioaccumulation by: Lepidium sativum and Sinapis alba plants. J Anal At Spectrom. Royal Society of Chemistry; 2016;31:2321–9.

17. Gomes MHF, Machado BA, Rodrigues ES, Montanha GS, Rossi ML, Otto R, et al. In Vivo Evaluation of Zn Foliar Uptake and Transport in Soybean Using X-ray Absorption and Fluorescence Spectroscopy. J Agric Food Chem. American Chemical Society; 2019;67:12172–81.

18. Schymura S, Fricke T, Hildebrand H, Franke K. Elucidating the Role of Dissolution in CeO_2 Nanoparticle Plant Uptake by Smart Radiolabeling. Angew Chemie Int Ed. Wiley-VCH Verlag; 2017;56:7411–4.

19. Peng C, Xu C, Liu Q, Sun L, Luo Y, Shi J. Fate and Transformation of CuO Nanoparticles in the Soil–Rice System during the Life Cycle of Rice Plants. Environ Sci Technol. American Chemical Society; 2017;51:4907–17.

20. Stegemeier JP, Schwab F, Colman BP, Webb SM, Newville M, Lanzirotti A, et al. Speciation Matters: Bioavailability of Silver and Silver Sulfide Nanoparticles to Alfalfa (*Medicago sativa*). Environ Sci Technol. American Chemical Society; 2015;49:8451–60.

21. Cifuentes Z, Custardoy L, de la Fuente JM, Marquina C, Ibarra MR, Rubiales D, et al. Absorption and translocation to the aerial part of magnetic carbon-coated nanoparticles through the root of different crop plants. J Nanobiotechnology. BioMed Central; 2010;8:26.

22. Serag MF, Kaji N, Venturelli E, Okamoto Y, Terasaka K, Tokeshi M, et al. Functional Platform for Controlled Subcellular Distribution of Carbon Nanotubes. ACS Nano. American Chemical Society; 2011;5:9264–70.

23. Wang Z, Xie X, Zhao J, Liu X, Feng W, White JC, et al. Xylem- and phloem-based transport of CuO nanoparticles in maize (Zea mays L.). Environ Sci Technol. American Chemical Society; 2012;46:4434–41.

24. Barrios AC, Rico CM, Trujillo-Reyes J, Medina-Velo IA, Peralta-Videa JR, Gardea-

674 Torresdey JL. Effects of uncoated and citric acid coated cerium oxide nanoparticles, bulk cerium
675 oxide, cerium acetate, and citric acid on tomato plants. Sci Total Environ. Elsevier B.V;
676 2016;563–564:956–64.
677 25. Wong MH, Misra RP, Giraldo JP, Kwak S-Y, Son Y, Landry MP, et al. Lipid Exchange
678 Envelope Penetration (LEEP) of Nanoparticles for Plant Engineering: A Universal Localization
679 Mechanism. Nano Lett. American Chemical Society; 2016;16:1161–72.
680 26. Sharma S, Sahu B, Srinivasan S, Singh M, Govindasamy J, Shanmugam V. Effect of
681 galvanotaxic graphene oxide on chloroplast activity: Interaction quantified with Biolayer-
682 Interferometry coupled confocal microscopy. Carbon. Elsevier Ltd; 2020;162:147–56.
683 27. Torney F, Trewyn BG, Lin VSY, Wang K. Mesoporous silica nanoparticles deliver DNA and
684 chemicals into plants. Nat Nanotechnol. Nature Publishing Group; 2007;2:295–300.
685 28. Vijayakumar PS, Abhilash OU, Khan BM, Prasad BL V. Nanogold-Loaded Sharp-Edged
686 Carbon Bullets as Plant-Gene Carriers. Adv Funct Mater. Wiley-VCH Verlag; 2010;20:2416–23.
687 29. Winkleman A, Gotesman G, Yoffe A, Naaman R. Immobilizing a Drop of Water:
688 Fabricating Highly Hydrophobic Surfaces that Pin Water Droplets. Nano Lett. American
689 Chemical Society; 2008;8:1241–5.
690 30. Dague E, Alsteens D, Latgé J-P, Verbelen C, Raze D, Baulard AR, et al. Chemical Force
691 Microscopy of Single Live Cells. Nano Lett. American Chemical Society; 2007;7:3026–30.
692 31. Wertz CF, Santore MM. Effect of surface hydrophobicity on adsorption and relaxation
693 kinetics of albumin and fibrinogen: Single-species and competitive behavior. Langmuir.
694 American Chemical Society; 2001;17:3006–16.
695 32. Jiang W, Tian Q, Vuong T, Shashaty M, Gopez C, Sanders T, et al. Comparison Study on
696 Four Biodegradable Polymer Coatings for Controlling Magnesium Degradation and Human
697 Endothelial Cell Adhesion and Spreading. ACS Biomater Sci Eng. American Chemical Society;
698 2017;3:936–50.
699 33. Hasan A, Pattanayek SK, Pandey LM. Effect of Functional Groups of Self-Assembled
700 Monolayers on Protein Adsorption and Initial Cell Adhesion. ACS Biomater Sci Eng. American
701 Chemical Society; 2018;4:3224–33.
702 34. Rasch MR, Rossinyol E, Hueso JL, Goodfellow BW, Arbiol J, Korgel BA. Hydrophobic
703 gold nanoparticle self-assembly with phosphatidylcholine lipid: Membrane-loaded and janus
704 vesicles. Nano Lett. American Chemical Society; 2010;10:3733–9.

705 35. Ungati H, Govindaraj V, Narayanan M, Mugesh G. Probing the Formation of a Seleninic
706 Acid in Living Cells by the Fluorescence Switching of a Glutathione Peroxidase Mimetic.
707 Angew Chemie - Int Ed. Wiley-VCH Verlag; 2019;58:8156–60.
708 36. Frankenberger WT, Engberg RA, Engberg RA. Effects of Selenium Supplementation of
709 Fertilizers on Human Nutrition and Selenium Status. CRC Press; 1998;103–20.
710 37. Pedrero Z, Madrid Y, Hartikainen H, Cámara C. Protective Effect of Selenium in Broccoli (
711 Brassica oleracea) Plants Subjected to Cadmium Exposure. J Agric Food Chem. American
712 Chemical Society; 2008;56:266–71.
713 38. Levard C, Hotze EM, Colman BP, Dale AL, Truong L, Yang XY, et al. Sulfidation of silver
714 nanoparticles: Natural antidote to their toxicity. Environ Sci Technol. American Chemical
715 Society; 2013;47:13440–8.
716 39. Wang Z, Zhang L, Zhao J, Xing B. Environmental processes and toxicity of metallic
717 nanoparticles in aquatic systems as affected by natural organic matter. Environ. Sci. Nano. Royal
718 Society of Chemistry; 2016. p. 240–55.
719 40. Teotia RS, Kalita D, Singh AK, Verma SK, Kadam SS, Bellare JR. Bifunctional
720 Polysulfone-Chitosan Composite Hollow Fiber Membrane for Bioartificial Liver. ACS Biomater
721 Sci Eng. American Chemical Society; 2015;1:372–81.
722 41. Lau C, Cooney MJ, Atanassov P. Conductive Macroporous Composite Chitosan−Carbon
723 Nanotube Scaffolds. Langmuir. American Chemical Society; 2008;24:7004–10.
724 42. Bordenave N, Grelier S, Pichavant F, Coma V. Water and moisture susceptibility of chitosan
725 and paper-based materials: Structure-property relationships. J Agric Food Chem. American
726 Chemical Society; 2007;55:9479–88.
727 43. USDA Economics, Statistics and Market Information System. Available from:
728 https://usda.library.cornell.edu/
729 44. Schilmiller AL, Howe GA. Systemic signaling in the wound response. Curr. Opin. Plant
730 Biol. Elsevier Ltd; 2005. p. 369–77.
731 45. Vijayakumar PS, Selvakumar S, Gholap RS, Singh AP, Prasad BLV. Vice to virtue:
732 Intracellular biogenic nanoparticles for the generation of carbon supported catalysts. J Nanosci
733 Nanotechnol. American Scientific Publishers; 2010. p. 905–11.
734 46. Anicuta S-G, Dobre L, Stroescu M, Jipa I. Fourier Transform Infrared (Ftir) Spectroscopy for
735 Characterization of Antimicrobial Films Containing Chitosan. 2010.

736 47. Li WP, Shanmugam V, Huang CC, Huang GD, Huang YK, Chiu SH, et al. Eccentric
737 inorganic-polymeric nanoparticles formation by thermal induced cross-linked esterification and
738 conversion of eccentricity to raspberry-like Janus. Chem Commun. Royal Society of Chemistry;
739 2013;49:1609–11.
740 48. Li Y, Bi J, Wang S, Zhang T, Xu X, Wang H, et al. Bio-inspired Edible Superhydrophobic
741 Interface for Reducing Residual Liquid Food. J Agric Food Chem. American Chemical Society;
742 2018;66:2143–50.
743 49. Jaggessar A, Shahali H, Mathew A, Yarlagadda PKDV. Bio-mimicking nano and micro-
744 structured surface fabrication for antibacterial properties in medical implants. J.
745 Nanobiotechnology. BioMed Central Ltd; 2017. p. 1–20.
746 50. Hernandez-Viezcas JA, Castillo-Michel H, Peralta-Videa JR, Gardea-Torresdey JL.
747 Interactions between CeO_2 Nanoparticles and the Desert Plant Mesquite: A Spectroscopy
748 Approach. ACS Sustain Chem Eng. American Chemical Society; 2016;4:1187–92.
749 51. Parsons JG, Lopez ML, Gonzalez CM, Peralta-Videa JR, Gardea-Torresdey JL. Toxicity and
750 biotransformation of uncoated and coated Nickel hydroxide nanoparticles on mesquite plants.
751 Environ Toxicol Chem. SETAC Press; 2010;29:1146–54.
752 52. Priester JH, Ge Y, Mielke RE, Horst AM, Moritz SC, Espinosa K, et al. Soybean
753 susceptibility to manufactured nanomaterials with evidence for food quality and soil fertility
754 interruption. Proc Natl Acad Sci U S A. National Academy of Sciences; 2012;109.
755 53. Liu Q, Chen B, Wang Q, Shi X, Xiao Z, Lin J, et al. Carbon Nanotubes as Molecular
756 Transporters for Walled Plant Cells. Nano Lett. American Chemical Society; 2009;9:1007–10.
757 54. Serag MF, Kaji N, Gaillard C, Okamoto Y, Terasaka K, Jabasini M, et al. Trafficking and
758 subcellular localization of multiwalled carbon nanotubes in plant cells. ACS Nano. American
759 Chemical Society; 2011;5:493–9.
760 55. Fernandes AN, Chen X, Scotchford CA, Walker J, Wells DM, Roberts CJ, et al. Mechanical
761 properties of epidermal cells of whole living roots of Arabidopsis thaliana: An atomic force
762 microscopy study. Phys Rev E - Stat Nonlinear, Soft Matter Phys. American Physical Society;
763 2012;85.
764 56. Dufrêne YF, Martínez-Martín D, Medalsy I, Alsteens D, Müller DJ. Multiparametric imaging
765 of biological systems by force-distance curve-based AFM. Nat. Methods. Nature Publishing
766 Group; 2013. p. 847–54.

767 57. Javier AM, Kreft O, Alberola AP, Kirchner C, Zebli B, Susha AS, et al. Combined atomic
768 force microscopy and optical microscopy measurements as a method to investigate particle
769 uptake by cells. Small. Wiley-VCH Verlag; 2006;2:394–400.
770 58. Zyuzin M V., Yan Y, Hartmann R, Gause KT, Nazarenus M, Cui J, et al. Role of the Protein
771 Corona Derived from Human Plasma in Cellular Interactions between Nanoporous Human
772 Serum Albumin Particles and Endothelial Cells. Bioconjug Chem. American Chemical Society;
773 2017;28:2062–8.
774 59. Yeo ELL, Cheah JUJ, Lim BY, Thong PSP, Soo KC, Kah JCY. Protein Corona around Gold
775 Nanorods as a Drug Carrier for Multimodal Cancer Therapy. ACS Biomater Sci Eng. American
776 Chemical Society; 2017;3:1039–50.
777 60. Abdelkhaliq A, Van Der Zande M, Punt A, Helsdingen R, Boeren S, Vervoort JJM, et al.
778 Impact of nanoparticle surface functionalization on the protein corona and cellular adhesion,
779 uptake and transport. J Nanobiotechnology. BioMed Central Ltd.; 2018;16:70.
780 61. Benabdellah K, Azcon-Aguilar C, Ferrol N. Soluble and membrane symbiosis-related
781 polypeptides associated with the development of arbuscular mycorrhizas in tomato
782 (Lycopersicon esculentum). New Phytol. Wiley-VCH Verlag; 1998;140:135–43.
783 62. Kaveh R, Li YS, Ranjbar S, Tehrani R, Brueck CL, Van Aken B. Changes in Arabidopsis
784 thaliana gene expression in response to silver nanoparticles and silver ions. Environ Sci Technol.
785 American Chemical Society; 2013;47:10637–44.
786 63. Pradas del Real AE, Vidal V, Carrière M, Castillo-Michel H, Levard C, Chaurand P, et al.
787 Silver Nanoparticles and Wheat Roots: A Complex Interplay. Environ Sci Technol. American
788 Chemical Society; 2017;51:5774–82.
789 64. Turakainen M, Hartikainen H, Seppänen MM. Effects of selenium treatments on potato
790 (Solanum tuberosum L.) growth and concentrations of soluble sugars and starch. J Agric Food
791 Chem. American Chemical Society; 2004;52:5378–82.
792 65. Xue T, Hartikainen H, Piironen V. Antioxidative and growth-promoting effect of selenium
793 on senescing lettuce. Plant Soil. Springer Publishing; 2001;237:55–61.
794 66. Sun X, Zhong Y, Huang Z, Yang Y. Selenium Accumulation in Unicellular Green Alga
795 Chlorella vulgaris and Its Effects on Antioxidant Enzymes and Content of Photosynthetic
796 Pigments. Cobine PA, editor. PLoS One. Public Library of Science; 2014;9:e112270.
797 67. Seppänen M, Turakainen M, Hartikainen H. Selenium effects on oxidative stress in potato.

798 Plant Sci. Elsevier Ireland Ltd; 2003;165:311–9.
799 68. Hartikainen H, Xue T, Piironen V. Selenium as an anti-oxidant and pro-oxidant in ryegrass.
800 Plant Soil. Springer Publishing; 2000;225:193–200.
801 69. Sharma S, Singh S, Ganguli AK, Shanmugam V. Anti-drift nano-stickers made of graphene
802 oxide for targeted pesticide delivery and crop pest control. Carbon. Elsevier Ltd; 2017;115:781–
803 90.
804 70. Roy Chowdhury S, Mondal S, Muthuraj B, Balaji SN, Trivedi V, Krishnan Iyer P.
805 Remarkably Efficient Blood-Brain Barrier Crossing Polyfluorene-Chitosan Nanoparticle
806 Selectively Tweaks Amyloid Oligomer in Cerebrospinal Fluid and Aβ1-40. ACS Omega.
807 American Chemical Society; 2018;3:8059–66.
808 71. Salehi H, Chehregani A, Lucini L, Majd A, Gholami M. Morphological, proteomic and
809 metabolomic insight into the effect of cerium dioxide nanoparticles to Phaseolus vulgaris L.
810 under soil or foliar application. Sci Total Environ. Elsevier B.V; 2018;616–617:1540–51.
811 72. Jarstfer AG, Farmer-Koppenol P, Sylvia DM. Tissue magnesium and calcium affect
812 arbuscular mycorrhiza development and fungal reproduction. Mycorrhiza. Springer Publishing;
813 1998;7:237–42.
814 73. Kitin P, Funada R, Sano Y, Ohtani J. Analysis by confocal microscopy of the structure of
815 cambium in the hardwood Kalopanax pictus. Ann Bot. Academic Press; 2000;86:1109–17.
816 74. Wu S, Baskin TI, Gallagher KL. Mechanical fixation techniques for processing and orienting
817 delicate samples, such as the root of Arabidopsis thaliana, for light or electron microscopy. Nat
818 Protoc. Nature Publishing Group; 2012;7:1113–24.
819 75. Dobrovolskaia MA, Patri AK, Zheng J, Clogston JD, Ayub N, Aggarwal P, et al. Interaction
820 of colloidal gold nanoparticles with human blood: effects on particle size and analysis of plasma
821 protein binding profiles. Nanomedicine Nanotechnology. Biol Med; 2009;5:106–17.
822 76. Majumdar S, Guha T, Kundu R. MTT Assay for Cytotoxicity Assessment in Oryza sativa
823 Root Tissue. BIO-PROTOCOL. Bio-Protocol, LLC; 2017;7.
824
825
826
827

Figures

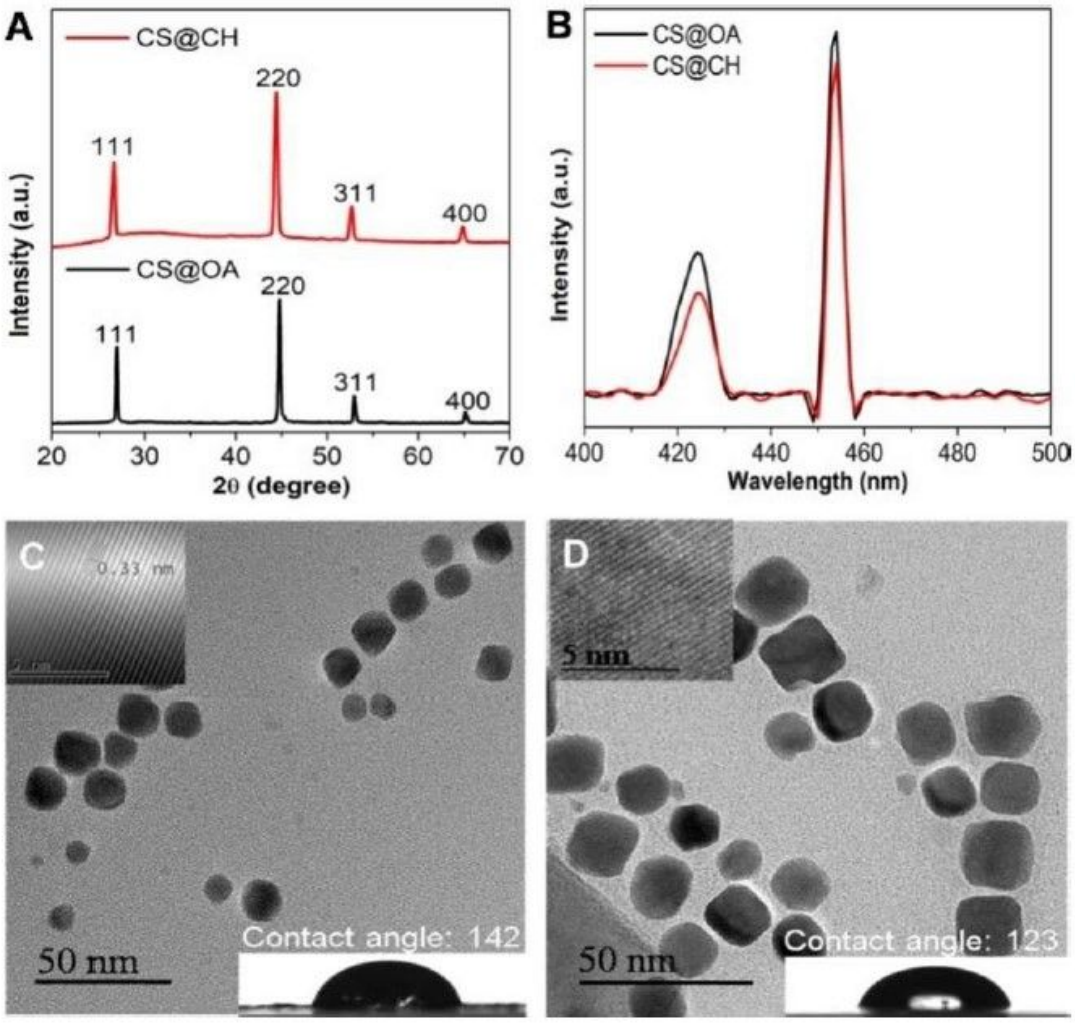

Figure 1

Characterization of the Cu2-xSe NPs (as-prepared oleylamine-coated CS@OA and chitosan-coated CS@CH). (A) XRD patterns of CS@OA (black curve) and CS@CH NPs (red curve). (B) PL spectra of CS@OA (black curve) and CS@CH (red curve) recorded at a 370 nm excitation wavelength. (C, D) TEM images of CS@OA and CS@CH showing the Cu2-xSe NPs, respectively (Inset (top left corner): HR-TEM images of the CS@OA and CS@CH NPs showing a 0.33 nm lattice spacing, corresponding to the (111) plane of Cu2-xSe) (Inset (bottom right corner): Contact angle on glass substrates coated with CS@OA or CS@CH NPs).

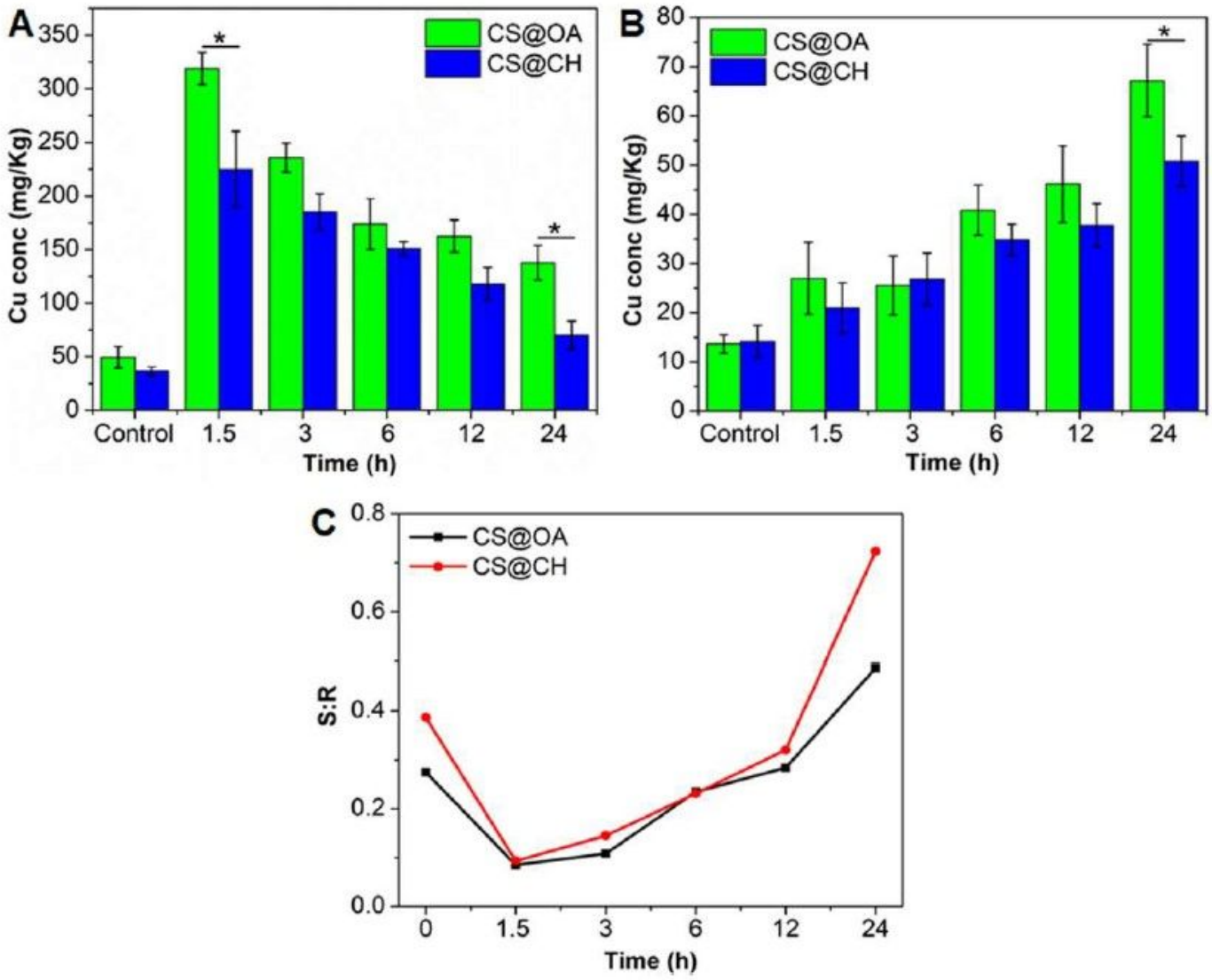

Figure 2

(A, B) Copper accumulation in the roots (A) and shoots (B) at different incubation times after spraying the roots with either CS@OA or CS@CH NPs estimated with ICP-MS (The copper concentration is normalised to per kg of root and shoot dry weight). (C) Shoot: root copper content ratio.

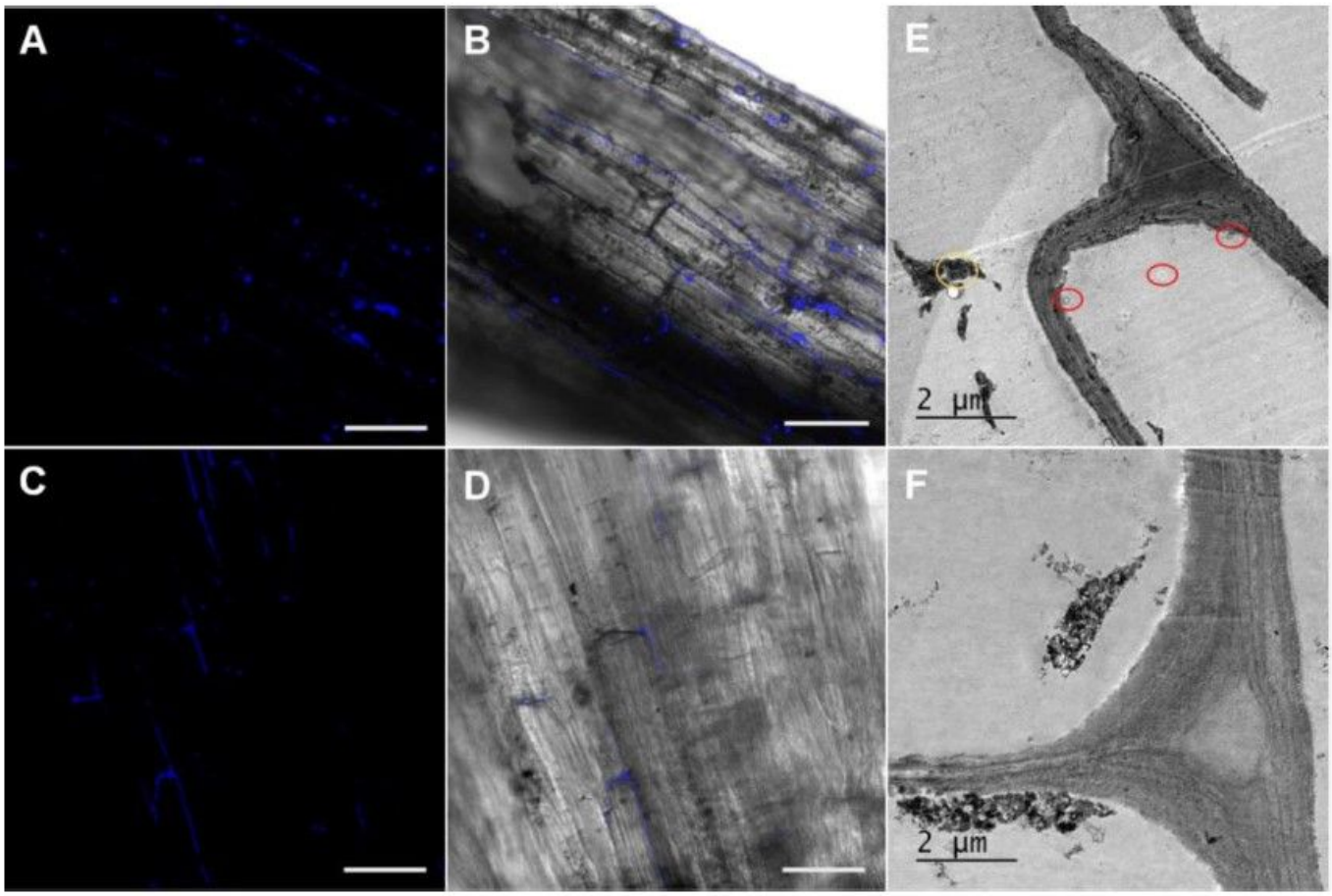

Figure 3

Confocal and TEM images of tomato plant tissue showing NPs uptake. 208 (A-D) show the confocal images of tomato roots sprayed with CS@OA (A, B) and CS@CH (C, D) NPs after 1 h of incubation time merged with the brightfield image (scale bar is 20 µM). (E, F) TEM images of the microtome sections of tomato roots sprayed with CS@OA (E) and CS@CH (F) after 3 h of incubation time.

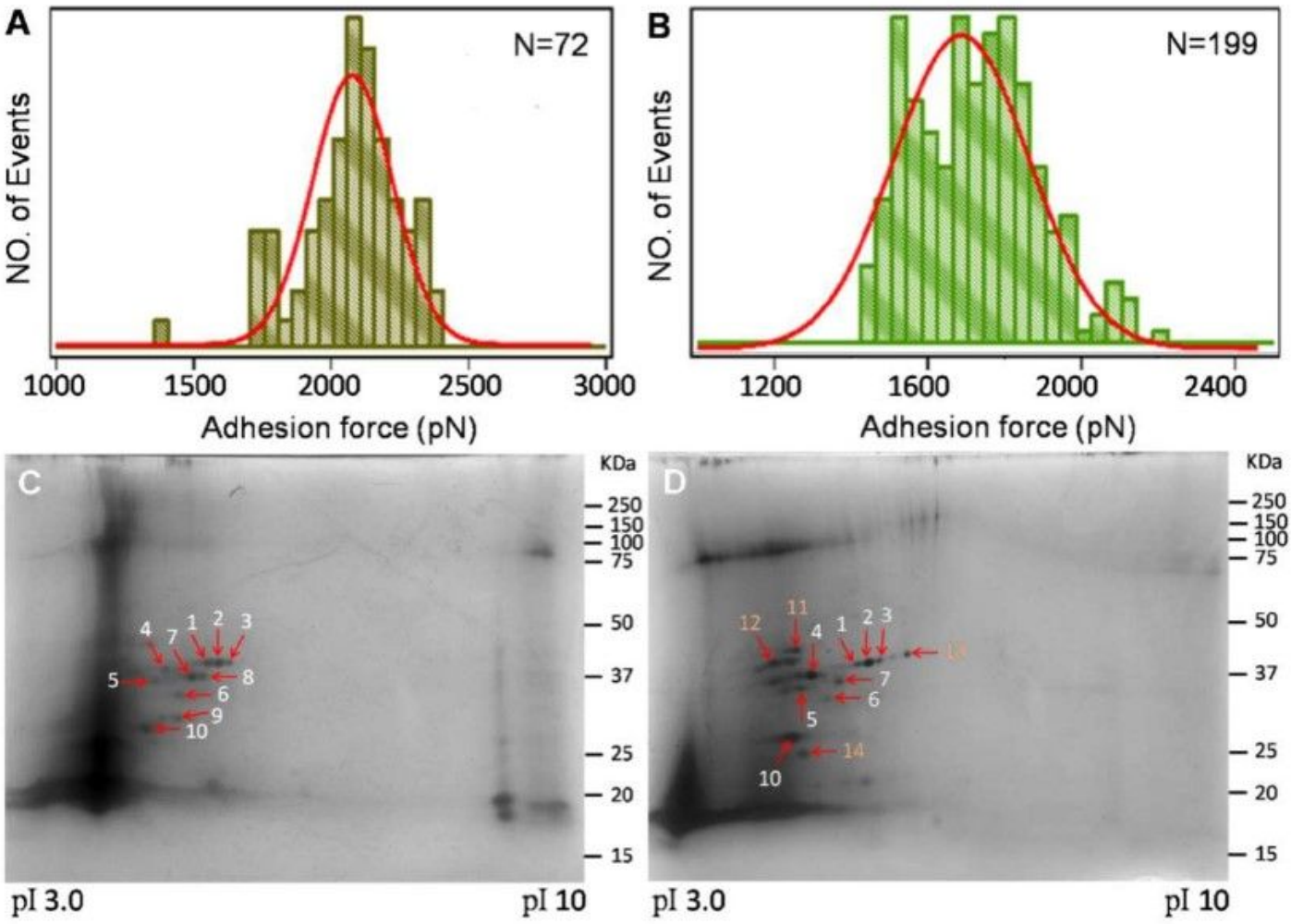

Figure 4

(A, B) Adhesion force between the root and an AFM tip modified with either CS@OA (A) or CS@CH (B) NPs in water. (C, D) 2D gel pattern of the protein corona extracted from roots with CS@OA (C) and CS@CH NPs (D) in a pH gradient of 3-10 with silver staining.

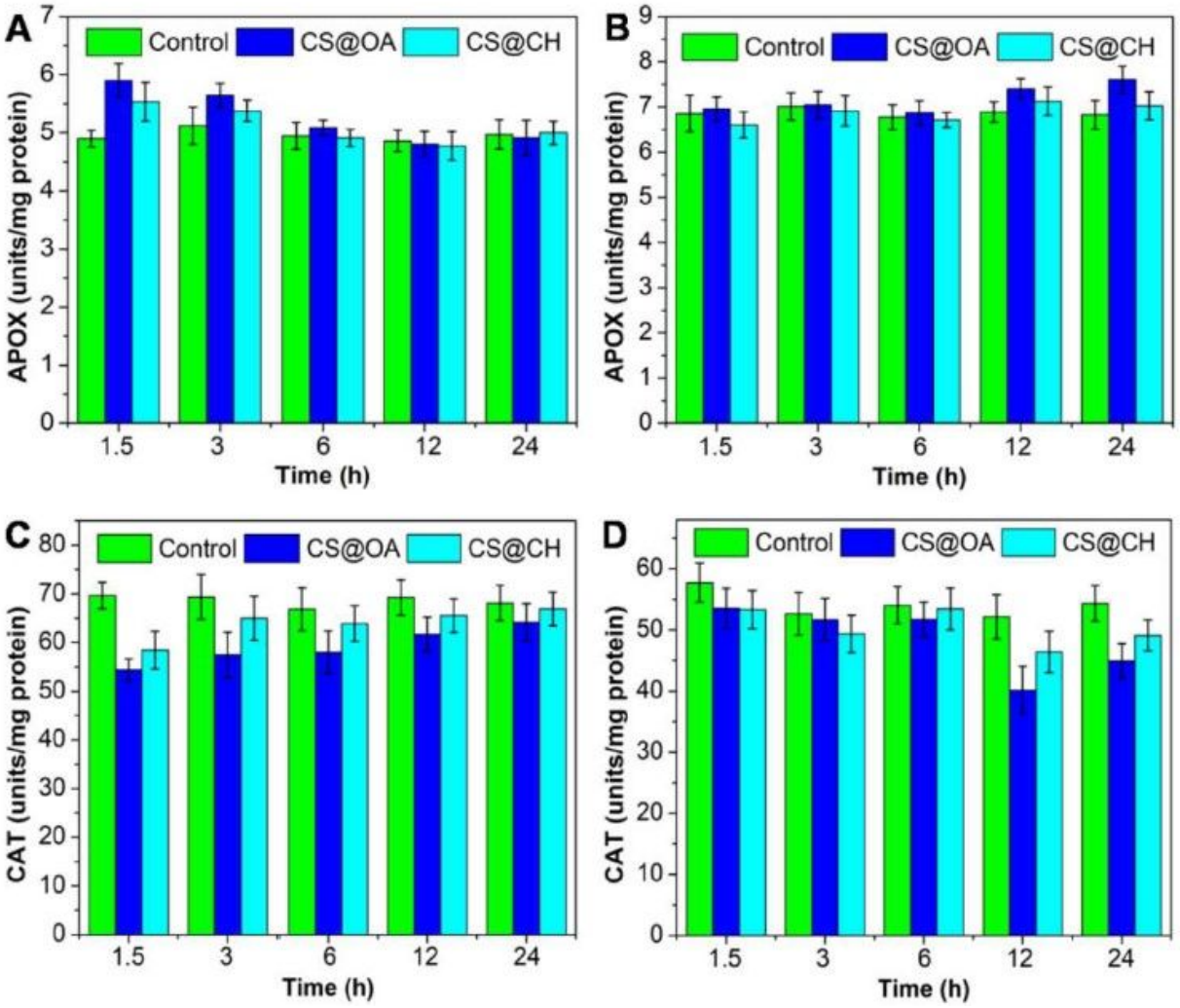

Figure 5

APOX and CAT antioxidant activity in tomato roots (A, C) and shoots (B, D) after exposure to Cu2-xSe (CS@OA and CS@CH) NPs compared to the control plants at different time points.

Supplementary Files

This is a list of supplementary files associated with this preprint. Click to download.

- Video2.avi
- TOC.tif
- Additionalfile1.docx
- video1.avi